This is a repository copy of *A new arc-length control method based on the rates of the internal and the dissipated energy*.

White Rose Research Online URL for this paper:
http://eprints.whiterose.ac.uk/100670/

Version: Accepted Version

A new arc-length control method based on the rates of the internal and the dissipated energy

Abstract

Purpose:
The purpose of this paper is to introduce a new arc-length control method for physically non-linear problems based on the rates of the internal and the dissipated energy.
Design/methodology/approach:
In this paper, the authors derive from the second law of thermodynamics the arc-length method based on the rate of the dissipated energy and from the time derivative of the energy density the arc-length method based on the rate of the internal energy.
Findings:
The method requires only two parameters and can automatically trace equilibrium paths which display multiple snap-back phenomena.
Originality/value:
A fully energy-based control procedure is developed, which facilitates switching between dissipative and non-dissipative arc-length control equations in a natural way. The method is applied to a plate with an eccentric hole using the phase field model for brittle fracture and to a perforated beam using interface elements with decohesion.

Keywords: arc-length control, path following technique, internal energy, dissipation

1. Introduction

Tracing an equilibrium path often requires an arc-length method due to the occurrence of (multiple) snap-through and snap-back phenomena. The arc-length method, developed originally in [1, 2] and cast in a format that is suitable for large-scale computations in [3, 4], works well for geometrically non-linear problems, but may fail to converge in case of physically non-linear problems due to strain localisation [5, 6]. To overcome this, an indirect displacement method was developed [6]. In this approach only degrees of freedom are considered that relate to the failure zone, and therefore requires an a priori knowledge of the expected failure zone.

The fact that physically non-linear problems can involve a monotonically increasing dissipation has been exploited in [7] and has been applied to damage models. The idea was further pursued and enhanced in [8] to plasticity models, and geometrically non-linear problems with damage. This class of arc-length methods switches from force control to arc-length control that is based on the dissipated energy when the increment of the dissipated energy reaches a critical value. A criterion for switching back from arc-length control to force control has been introduced in [8]. In this paper, a new

formulation is proposed which switches between the internal energy and the dissipated energy and hence, is completely based on energy. During the entire loading process the increment of the internal energy is computed and in the elastic regime an internal energy based arc-length control is used. The present path-following method requires only two parameters for tracing an entire equilibrium path and is especially robust when the equilibrium path exhibits several several snap-through and/or snap-back phenomena.

2. Arc-length control based on the rates of the internal and the dissipated energy

This section introduces a novel arc-length control method which is based on the rates of the internal and the dissipated energy.

2.1. Necessity of arc-length control

The state of a solid is governed by the equilibrium of external and internal forces

$$\underline{f}^{\text{int}}(\underline{u}) = \underline{f}^{\text{ext}} \tag{1}$$

where the external force vector can be represented by a normalised load vector $\underline{\hat{f}}$ and the loading parameter λ, as follows

$$\underline{f}^{\text{ext}} = \lambda \underline{\hat{f}}. \tag{2}$$

Neither force control, nor displacement control is in general suitable for tracing the entire equilibrium path. During force control, the loading parameter λ is prescribed, while for a displacement control, the displacement u is prescribed for some points of the solid, see Fig. 1 for a typical force-displacement curve.
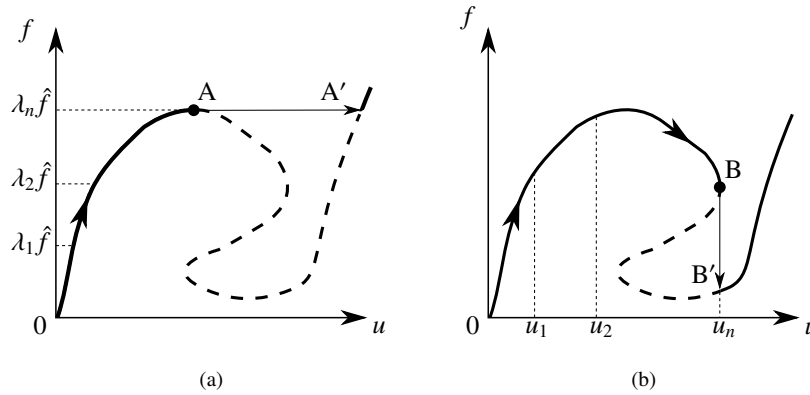

Figure 1: (a) Force control is not able to capture the dashed equilibrium path between the points A and A′ (snap-through). (b) Displacement control is unable to trace the dashed equilibrium path between the points B and B′ (snap-back).

Up to point A in Fig. 1(a) force control, which is then monotonically increasing, can be employed

$$\lambda_1 < \lambda_2 < \ldots < \lambda_n, \tag{3}$$

2

whereas up to point B in Fig. 1(b) displacement control can be used,

$$u_1 < u_2 < \ldots < u_n. \tag{4}$$

However, force control is not able to capture the snap-through after the peak load at point A, while displacement control is unable to capture the snap-back behaviour at point B. Therefore, an arc-length control is necessary in order to properly trace the equilibrium path during loading. An arc-length control adds an additional constraint equation to Eq. (1), $\varphi = \varphi(\underline{u}, \lambda)$, which ensures that the equilibrium path can be followed. By adding the additional constraint equation, the following system of equations must be solved

$$\underline{H}(\underline{u}, \lambda) = \begin{bmatrix} \underline{f}^{\text{int}}(\underline{u}) - \lambda \underline{\hat{f}} \\ \varphi(\underline{u}, \lambda) \end{bmatrix} = \begin{bmatrix} \underline{0} \\ 0 \end{bmatrix}. \tag{5}$$

Assuming that the solution in the $n+1$-th increment and i-th iteration is known, $\underline{u}_{n+1}^i$ and λ_{n+1}^i, Eq. (5) can be linearised using a TAYLOR series around $\underline{u}_{n+1}^i$, λ_{n+1}^i, as follows

$$\underline{H}(\underline{u}, \lambda) \approx \underline{H}(\underline{u}_{n+1}^i, \lambda_{n+1}^i) + \underline{\underline{K}}_T(\underline{u}_{n+1}^i, \lambda_{n+1}^i) \cdot \begin{bmatrix} \underline{u} - \underline{u}_{n+1}^i \\ \lambda - \lambda_{n+1}^i \end{bmatrix} = \underline{0} \tag{6}$$

with

$$\underline{\underline{K}}_T(\underline{u}, \lambda) = \begin{bmatrix} \dfrac{\partial \underline{f}^{\text{int}}(\underline{u})}{\partial \underline{u}} & -\underline{\hat{f}} \\ \dfrac{\partial \varphi(\underline{u}, \lambda)}{\partial \underline{u}} & \dfrac{\partial \varphi(\underline{u}, \lambda)}{\partial \lambda} \end{bmatrix} = \begin{bmatrix} \underline{\underline{K}} & -\underline{\hat{f}} \\ \underline{v}^T & w \end{bmatrix}. \tag{7}$$

The solution for $\underline{u}_{n+1}^{i+1}$, λ_{n+1}^{i+1} in the $n+1$-th increment in the $i+1$-th iteration in Eq. (6), $\underline{H}(\underline{u}_{n+1}^{i+1}, \lambda_{n+1}^{i+1}) = \underline{0}$, then follows from

$$\begin{bmatrix} \underline{u} \\ \lambda \end{bmatrix}_{n+1}^{i+1} = \begin{bmatrix} \underline{u} \\ \lambda \end{bmatrix}_{n+1}^{i} - \underline{\underline{K}}_T^{-1} \Big|_{n+1}^{i} \cdot \begin{bmatrix} \underline{f}^{\text{int}}(\underline{u}) - \lambda \underline{\hat{f}} \\ \varphi(\underline{u}, \lambda) \end{bmatrix}_{n+1}^{i}. \tag{8}$$

To increase efficiency, the inverse of the matrix $\underline{\underline{K}}_T$ can be evaluated exploiting the SHERMAN-MORRISON formula, see Appendix A.

2.2. Arc-length control based on the rate of dissipated energy

An arc-length function based on the rate of dissipated energy has been introduced in [7]. The procedure uses a force control at the beginning of the loading, and when the dissipated energy reaches a certain limit switches to dissipation-based arc-length control. The dissipation-based arc-length control is motivated by the fact that during loading the amount of dissipated energy can only increase monotonically. Therefore, by prescribing the amount of energy which should be dissipated in each loading step, the equilibrium path can be traced automatically.

The first law of thermodynamics gives a statement about the conservation of energy – energy can neither be destroyed nor created. However, the first law of thermodynamics does not give a statement about the dissipative nature of a process. The dissipative

3

behaviour of a process can be described by the second law of thermodynamics. In a *local* form for a constant temperature [9], the second law of thermodynamics reads

$$\dot{\mathcal{D}} = \sigma_{ij}\dot{\varepsilon}_{ij} - \dot{\psi} \geq 0 \tag{9}$$

where $\dot{\mathcal{D}}$ is the dissipation and ψ the energy density. We now assume that for the constitutive behaviour between the stress σ_{ij} and the strain ε_{ij} a damage law of the form

$$\sigma_{ij}(\varepsilon_{ij}, d) = g(d)C_{ijkl}\varepsilon_{kl} \tag{10}$$

is used with the damage parameter $d \in [0, 1]$ (0: undamaged state, 1: fully broken state), the degradation function $g(d)$ and the elasticity tensor equipped with the usual major and minor symmetries: $C_{ijkl} = C_{jikl}, C_{ijkl} = C_{ijlk}, C_{ijkl} = C_{klij}$. The energy density ψ then reads

$$\psi(\varepsilon_{ij}, d) = \frac{1}{2}\sigma_{ij}(\varepsilon_{ij}, d)\varepsilon_{ij} \tag{11}$$

so that

$$\frac{\partial\psi}{\partial\varepsilon_{kl}} = \frac{1}{2}\frac{\partial\sigma_{ij}}{\partial\varepsilon_{kl}}\varepsilon_{ij} + \frac{1}{2}\sigma_{ij}\frac{\partial\varepsilon_{ij}}{\partial\varepsilon_{kl}} = \frac{1}{2}g(d)C_{ijkl}\varepsilon_{ij} + \frac{1}{2}g(d)C_{ijkl}\varepsilon_{kl}\delta_{ik}\delta_{jl}$$
$$= g(d)C_{ijkl}\varepsilon_{ij} = g(d)C_{klij}\varepsilon_{ij} = \sigma_{kl}. \tag{12}$$

There are two ways to elaborate the time derivative of the energy density ψ in Eq. (9). The first option is to use the chain rule with Eq. (12)

$$\dot{\psi} = \frac{\partial\psi}{\partial\varepsilon_{ij}}\dot{\varepsilon}_{ij} + \frac{\partial\psi}{\partial d}\dot{d} = \sigma_{ij}\dot{\varepsilon}_{ij} + \frac{\partial\psi}{\partial d}\dot{d} \tag{13}$$

which yields

$$\dot{\mathcal{D}} = -\frac{\partial\psi}{\partial d}\dot{d} \geq 0. \tag{14}$$

The second option is to apply the product rule

$$\dot{\psi} = \frac{1}{2}\dot{\sigma}_{ij}\varepsilon_{ij} + \frac{1}{2}\sigma_{ij}\dot{\varepsilon}_{ij} \tag{15}$$

which results in

$$\dot{\mathcal{D}} = \frac{1}{2}\sigma_{ij}\dot{\varepsilon}_{ij} - \frac{1}{2}\dot{\sigma}_{ij}\varepsilon_{ij} \geq 0. \tag{16}$$

Assuming that there are no discontinuities in the solid, the *global* forms of Eq. (14) and Eq. (16) can be written as

$$\dot{\mathcal{E}}^D = \int \dot{\mathcal{D}}\,\mathrm{dV} = \int_\Omega \frac{1}{2}\sigma_{ij}\dot{\varepsilon}_{ij} - \frac{1}{2}\dot{\sigma}_{ij}\varepsilon_{ij}\,\mathrm{dV} = \int_\Omega -\frac{\partial\psi}{\partial d}\dot{d}\,\mathrm{dV} \tag{17}$$

where $\dot{\mathcal{E}}^D$ is the rate of dissipated energy. It can be observed from Eq. (17) that $\dot{\mathcal{E}}^D$ directly follows from the evolution of the damage variable d. It is noted that the dissipated energy $\mathcal{E}^D$ increases monotonically, since $\dot{\mathcal{E}}^D \geq 0$ follows from $\dot{d} \geq 0$ and $\frac{\partial\psi}{\partial d} \leq 0$ in Eq. (17).

The second integral in Eq. (17) can be expressed in matrix-vector format using

$$\underline{\boldsymbol{\varepsilon}} = \underline{\underline{\mathbf{B}}}\,\underline{\boldsymbol{u}}, \tag{18}$$

Eq. (1), and Eq. (2) as

$$\dot{\mathcal{E}}^D = \int_\Omega \frac{1}{2}\dot{\underline{\boldsymbol{u}}}^T \underline{\underline{\mathbf{B}}}^T \underline{\boldsymbol{\sigma}}\,\mathrm{dV} - \int_\Omega \frac{1}{2}\underline{\boldsymbol{u}}^T \underline{\underline{\mathbf{B}}}^T \dot{\underline{\boldsymbol{\sigma}}}\,\mathrm{dV}$$

$$= \frac{1}{2}\dot{\underline{\boldsymbol{u}}}\,\underline{\boldsymbol{f}}^{\text{int}}(\underline{\boldsymbol{u}}) - \frac{1}{2}\underline{\boldsymbol{u}}\,\dot{\underline{\boldsymbol{f}}}^{\text{int}}(\underline{\boldsymbol{u}}) = \frac{1}{2}\dot{\underline{\boldsymbol{u}}}\lambda\hat{\underline{\boldsymbol{f}}} - \frac{1}{2}\underline{\boldsymbol{u}}\dot{\lambda}\hat{\underline{\boldsymbol{f}}}. \tag{19}$$

Replacing $\dot{\mathcal{E}}^D$ in Eq. (19) with the rate of the path parameter $\dot{\tau}^D$ yields

$$\frac{1}{2}(\lambda\dot{\underline{\boldsymbol{u}}}^T - \dot{\lambda}\underline{\boldsymbol{u}}^T)\hat{\underline{\boldsymbol{f}}} - \dot{\tau}^D = 0. \tag{20}$$

Any time discretisation scheme would result in

$$\frac{1}{2}\left(\lambda_n\underline{\boldsymbol{u}}_{n+1}^T - \lambda_{n+1}\underline{\boldsymbol{u}}_n^T\right)\hat{\underline{\boldsymbol{f}}} - \Delta\tau^D = 0, \tag{21}$$

see Appendix B.2. It is noted that the time discretisation of the last term in Eq. (17) is in general not equal to Eq. (21), although the second and the third integrals in Eq. (21) are equal from a continuity perspective. Eq. (21) can now be used as the constraint equation in Eq. (5) and attains the following form

$$\varphi^D(\underline{\boldsymbol{u}}, \lambda) = \frac{1}{2}\left(\lambda_n\underline{\boldsymbol{u}}^T - \lambda\underline{\boldsymbol{u}}_n^T\right)\hat{\underline{\boldsymbol{f}}} - \Delta\tau^D. \tag{22}$$

The parameter $\Delta\tau^D$ in Eq. (22) can be interpreted as the prescribed step size for each increment – it prescribes the amount of energy which needs to be dissipated in one increment.

2.3. Arc-length control based on the rate of the internal energy

Now, a new arc-length function will be introduced for the regime when the rate of dissipated energy $\dot{\mathcal{E}}^D$ due to the evolution of the damage variable d is very small, e.g., at the onset of loading. Again assuming that there are no discontinuities in the solid, and using Eq. (1), Eq. (2) and Eq. (18), we can write Eq. (15) in the *global* form to yield the rate of the internal energy $\dot{\mathcal{U}}$ in matrix-vector form

$$\dot{\mathcal{U}} = \int_\Omega \dot{\psi}\,\mathrm{dV} = \int_\Omega \frac{1}{2}\dot{\underline{\boldsymbol{u}}}^T \underline{\underline{\mathbf{B}}}^T \underline{\boldsymbol{\sigma}} + \frac{1}{2}\underline{\boldsymbol{u}}^T \underline{\underline{\mathbf{B}}}^T \dot{\underline{\boldsymbol{\sigma}}}\,\mathrm{dV}$$

$$= \frac{1}{2}\dot{\underline{\boldsymbol{u}}}^T \underline{\boldsymbol{f}}^{\text{int}}(\underline{\boldsymbol{u}}) + \frac{1}{2}\underline{\boldsymbol{u}}^T \dot{\underline{\boldsymbol{f}}}^{\text{int}}(\underline{\boldsymbol{u}}) = \frac{1}{2}\left(\dot{\underline{\boldsymbol{u}}}^T \lambda + \underline{\boldsymbol{u}}^T \dot{\lambda}\right)\hat{\underline{\boldsymbol{f}}}. \tag{23}$$

Replacing $\dot{\mathcal{U}}$ with the path parameter $\dot{\tau}^U$ in Eq. (16) and applying the midpoint rule (see Appendix B.1) results in

$$\frac{1}{2}\left(\lambda_{n+1}\underline{\boldsymbol{u}}_{n+1}^T - \lambda_n\underline{\boldsymbol{u}}_n^T\right)\hat{\underline{\boldsymbol{f}}} - \Delta\tau^U = 0 \tag{24}$$

which can be used as a constraint equation in Eq. (5), as follows

$$\varphi^U(\underline{\mathbf{u}}, \lambda) = \frac{1}{2}\left(\lambda\underline{\mathbf{u}}^T - \lambda_n\underline{\mathbf{u}}_n^T\right)\hat{\underline{\mathbf{f}}} - \Delta\tau^U. \tag{25}$$

The parameter $\Delta\tau^U$ in Eq. (25) can be interpreted as the prescribed step size for an increment – it prescribes the amount of internal energy which needs to be introduced into the system in one increment.

In the first iteration ($i=1$) of the first increment ($n=1$)

$$\left.\frac{\partial\varphi^U(\underline{\mathbf{u}}, \lambda)}{\partial\lambda}\right|_{n=1}^{i=1} = \left.\frac{1}{2}\underline{\mathbf{u}}^T\hat{\underline{\mathbf{f}}}\right|_{n=1}^{i=1} = \frac{1}{2}\underline{\mathbf{u}}_1^{1T}\hat{\underline{\mathbf{f}}} = 0, \tag{26}$$

and Eq. (7) would result in a singular matrix with $\underline{\mathbf{u}}_1^1 = \underline{\mathbf{u}}_0 = \underline{\mathbf{0}}$. Hence, in the first increment $n=1$ the following arc-length expression is used

$$\varphi_1^F(\lambda) = \lambda - \Delta\tau_1^F, \qquad \left.\frac{\partial\varphi_1^F(\lambda)}{\partial\lambda}\right|_{n=1} = 1 \tag{27}$$

which is equivalent to force control. After the first increment, the solution for $\underline{\mathbf{u}}_1$ and λ_1 is known. From the solution for $\underline{\mathbf{u}}_1$ and λ_1 the rate of the internal energy for the first increment $\Delta\tau_1^U$ can be evaluated using Eq. (25),

$$\Delta\tau_1^U = \frac{1}{2}\left(\lambda_1\underline{\mathbf{u}}_1^T - \lambda_0\underline{\mathbf{u}}_0^T\right)\hat{\underline{\mathbf{f}}} = \frac{1}{2}\lambda_1\underline{\mathbf{u}}_1^T\hat{\underline{\mathbf{f}}}. \tag{28}$$

$\Delta\tau_1^U$ from Eq. (28) can then be used in the following increments as the prescribed step size. An adaptive step size scheme could be applied as in [7]. However, for the examples in Section 3 no adaptive step size scheme has been used.

Next to $\Delta\tau_1^F$ a ratio a needs to be defined. This parameter specifies when the load control has to switch from internal energy based arc-length control to dissipation based arc-length control and is defined as

$$a = \frac{\Delta\tau^D}{\Delta\tau^U}. \tag{29}$$

When the force-displacement curve exhibits a more brittle behaviour – i. e. little damage occurs before the maximum peak force – the parameter a typically must be assigned a smaller value. If a is chosen too large the simulation cannot switch to the dissipation based arc-length control and will not find an equilibrium at a snap-through / snap-back. For a too small a, we switch too early to the dissipation based arc-length control. In order to determine a, one can start a simulation with a large a. Then, we can assign a value to a that is smaller than the term $\frac{\Delta\tau^D}{\Delta\tau^U}$ from the last increment where an equilibrium could be found. The algorithm is summarised in Algorithm 1.

A simulation starts with a prescribed step size for the force $\Delta\tau_1^F$, which gives a step size $\Delta\tau_1^U$ for the rate of internal energy at point C, cf. Fig. 2. $\Delta\tau_1^U$ is then used as the prescribed step size for the arc-length control φ^U based on the rate of internal energy from point C to D, $\Delta\tau^U = \Delta\tau_1^U$. If, at the end of an increment, the incremental dissipated energy times the ratio factor a is larger than the prescribed increment for the

Algorithm 1: Algorithm for the loading process for arc-length control based on the rate of internal energy $\dot{\mathcal{U}}$ and the rate of the dissipated energy $\dot{\mathcal{E}}^D$

internal energy $\Delta\tau^D > a\Delta\tau^U = a\Delta\tau_1^U$ (point D in Fig. 2), the loading process switches from internal energy based (φ^U) to dissipation based (φ^D) arc-length control with a pre-
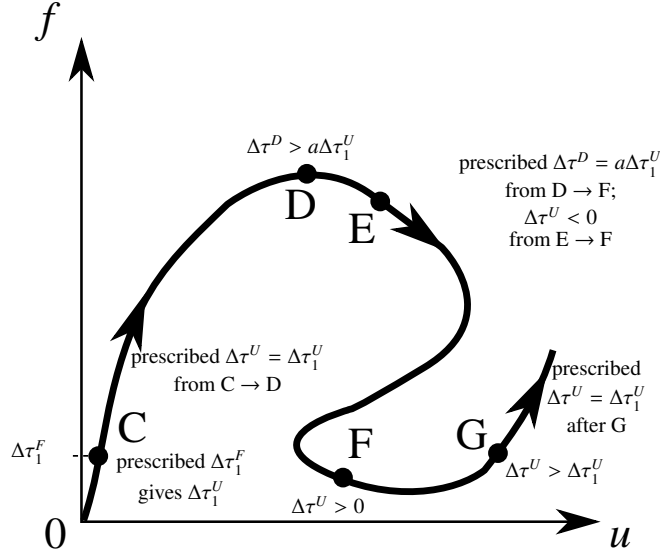
Figure 2: Path following technique using an arc-length control which is based on the rate of internal energy $\dot{\mathcal{U}}$ and the rate of dissipated energy $\dot{\mathcal{E}}^D$. Switch from rate of internal energy based arc-length control φ^U to dissipation based arc-length control φ^D at point D; switch from dissipation based arc-length control φ^D to internal energy based arc-length control φ^U at point G.

scribed step size $\Delta\tau^D = a\Delta\tau_1^U$. The increment in the internal energy becomes negative, $\Delta\tau^U < 0$, between point E and F Fig. 2. When the incremental internal energy $\Delta\tau^U$ becomes again larger than $\Delta\tau_1^U$ (point G in Fig. 2), the loading process switches back to an internal energy based arc-length control φ^U with a prescribed step size $\Delta\tau^U = \Delta\tau_1^U$. It is emphasised that the arc-length method requires just two parameters: $\Delta\tau_1^F$ and a.

3. Numerical examples

In this section two numerical examples are considered.

3.1. Phase field model for brittle fracture

We consider the phase field problem for brittle fracture governed by the equations

$$\sigma_{ij,i} = 0, \tag{30}$$

$$\frac{\mathcal{G}_c}{2\ell}[d - 4\ell^2\Delta d] + \frac{\partial g}{\partial d}\mathcal{H} = 0 \tag{31}$$

and subject to the boundary conditions

$$\sigma_{ij}n_j = h_i \text{ on } \partial\Omega_h, \tag{32}$$

$$u_i = \bar{u}_i \text{ on } \partial\Omega_u, \tag{33}$$

$$d_{,i}n_i = 0 \text{ on } \partial\Omega \tag{34}$$

8

the boundary $\partial\Omega$ decomposed into the parts $\partial\Omega_h$ and $\partial\Omega_u$ ($\partial\Omega_h \cap \partial\Omega_u = \emptyset$, $\partial\Omega_h \cup \partial\Omega_u = \partial\Omega$), the prescribed surface traction $\underline{h}$ and prescribed displacement $\underline{\bar{u}}$. $\mathcal{H}$ denotes the history field

$$\mathcal{H} = \max \psi \tag{35}$$

which was introduced in [10] in order to ensure irreversibility of the phase field variable d. It is noted that ψ is the energy density for the damaged solid

$$\psi = g(d)\psi^{\text{el}} \tag{36}$$

where ψ^{el} corresponds to the energy density for the undamaged solid

$$\psi^{\text{el}} = \frac{1}{2}\lambda\varepsilon_{ii}\varepsilon_{jj} + \mu\varepsilon_{ij}\varepsilon_{ij}. \tag{37}$$

The following degradation function $g(d)$ is used

$$g(d) = (1 - d)^2. \tag{38}$$

The dissipated energy is given by

$$\dot{\mathcal{E}}^D = \int_\Omega \mathcal{G}_c\dot{\gamma}_\ell \, \mathrm{dV} \tag{39}$$

with the crack surface density function

$$\gamma_\ell = \frac{1}{4\ell}\left(d^2 + 4\ell^2 d_{,i}d_{,i}\right). \tag{40}$$

Recalling Eq. (17) gives

$$\dot{\mathcal{E}}^D = \int_\Omega -\frac{\partial\psi}{\partial d}\dot{d} \, \mathrm{dV} = \int_\Omega \mathcal{G}_c\dot{\gamma}_\ell \, \mathrm{dV}, \tag{41}$$

i. e. the energy which is dissipated in the bulk is equal to the energy dissipated upon propagation of the smeared crack surface.

The material parameters are $E = 210 \, \mathrm{N/mm}^2$, $\nu = 0.3$, $\mathcal{G}_c = 2.7 \times 10^{-3} \, \mathrm{N/mm}$, and the length scale parameter is $\ell = 0.02$ mm. Plane strain is assumed. The two parameters for the arc-length control are $\Delta\tau_1^F = 0.2$ N and $a = 0.25$. The phase field problem for brittle fracture is applied to the plate with the eccentric hole in Fig. 3 which has been considered with different dimensions in [11]. The mesh consists of 9494 linear quads which gives the mesh size $h \approx 0.01$ mm. The force displacement curve and the development of the phase field variable d are shown in Fig. 4 and Fig. 5.

For the phase field for brittle fracture, nucleation can occur in the absence of stress singularities. However, the nucleation stress is related to the length scale parameter ℓ. This has been addressed in [12, 13]. Furthermore, [14] showed that Γ-convergence is not attained numerically for the phase field model for brittle fracture.
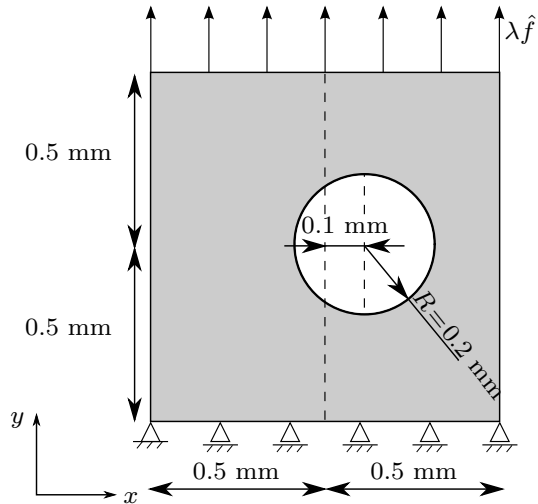
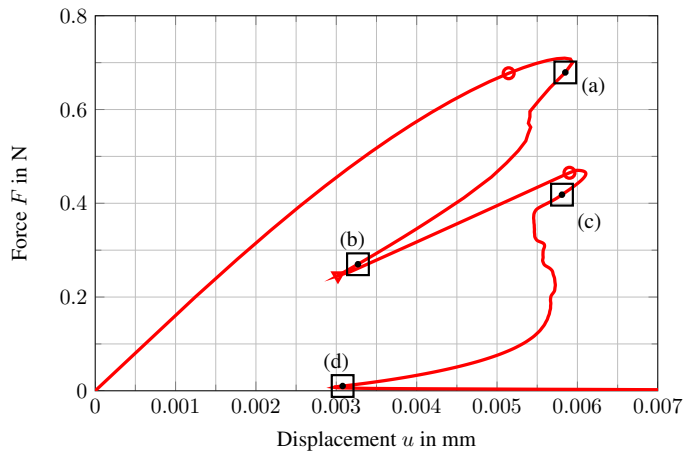Figure 3: Plate under tension with an eccentric hole.

Figure 4: Force-displacement curve for the plate under tension with an eccentric hole with mesh size $h \approx 0.01$ mm and length scale parameter $\ell = 0.02$ mm. Circles denote the switch from internal energy to dissipation based arc-length control, the triangle denotes the switch from dissipation to internal energy based arc-length control. Squares correspond to the phase field distributions for d in Fig. 5.

3.2. Perforated beam with interface elements

As a second numerical example, we consider the perforated beam depicted in Fig. 6(a). We take the same material parameters as in [8], $E = 100$ N/mm^2, $\nu = 0.3$, $\mathcal{G}_c = 2.5 \times 10^{-3}$ N/mm. For the cohesive interface, a bi-linear cohesive law with ultimate traction $t_{\text{ult}} = 1$ N/mm^2 and the dummy stiffness $k = 10^4$ N/mm^3 is applied
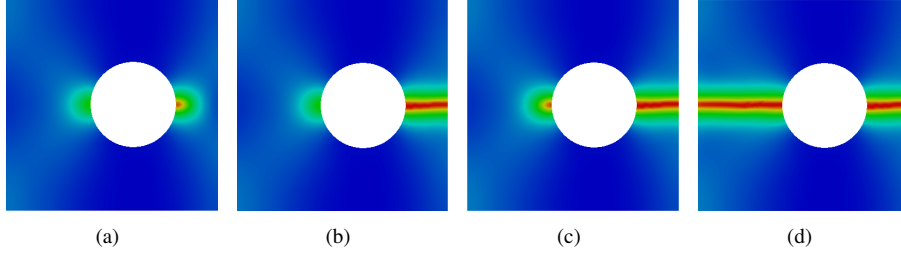
Figure 5: Propagation of the phase field variable d for the plate with an eccentric hole under tension; plots correspond to the squares in Fig. 4
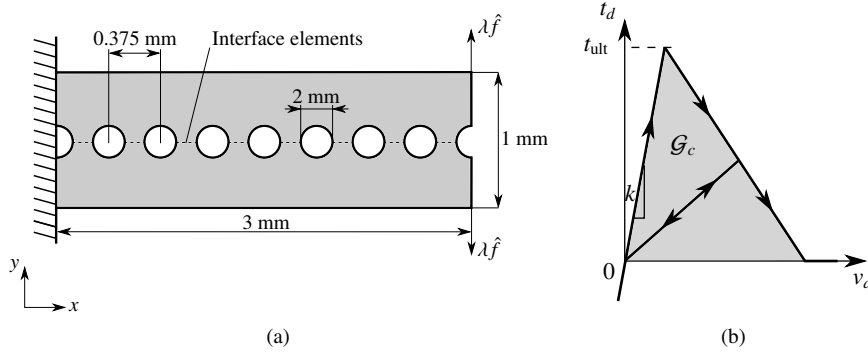

Figure 6: (a) Set-up for the perforated beam. (b) Bi-linear cohesive law for the interface elements. The shaded grey area is equivalent to the fracture toughness $\mathcal{G}_c$.

to the interface elements, cf. Fig. 6(b). 15354 linear triangular elements are used and along the interface a two-point Newton-Cotes integration scheme is used in order to avoid stress oscillations along the interface [15], see also [16] for a discussion on the integration of interface elements in an isogeometric context. The two parameters for the arc-length control are $\Delta\tau_1^F = 0.025$ N and $a = 0.1$.

The bulk is assumed to be linear elastic; no damage law is used. Energy is only dissipated in the interface elements, so that the dissipated energy in Eq. (17) becomes

$$\dot{\mathcal{E}}^D = \int_\Omega \frac{1}{2}\sigma_{ij}\dot{\varepsilon}_{ij} - \frac{1}{2}\dot{\sigma}_{ij}\varepsilon_{ij} \, \mathrm{dV} = \int_\Gamma \frac{1}{2}t_i\dot{v}_i - \frac{1}{2}\dot{t}_iv_i \, \mathrm{dA}. \tag{42}$$

The ensuing force-displacement curve is given in Fig. 7.

4. Concluding remarks

A proper control of the non-linear process is crucial in computational solid mechanics. During the past thirty years the Riks-Wempner arc-length or path-following
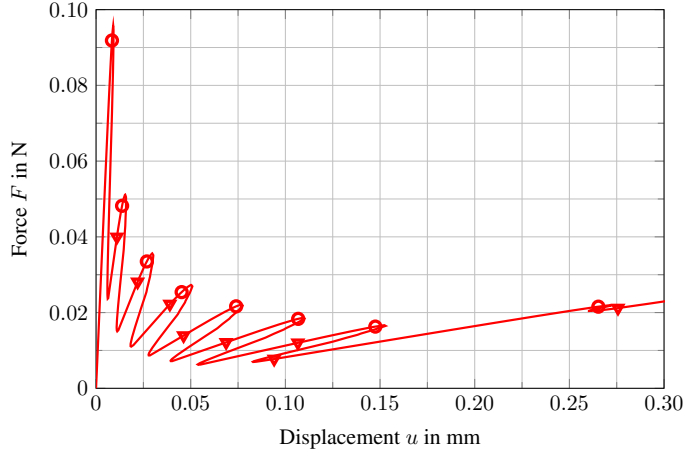
Figure 7: Force-displacement curve for the perforated beam; circles denote the switch from internal energy to dissipation based arc-length control, triangles denote the switch from dissipation to internal energy based arc-length control.

method [1, 2] has become the standard, as it is able to overcome snap-back and snap-through behaviour which can be inherent in equilibrium paths under quasi-static loadings. Originally applied predominantly to geometrically non-linear behaviour of slender structures, it is nowadays applied in any situation where severe non-linearities play a role, including plasticity and damage, and concomitant strain localisation phenomena. The latter type of non-linearities are very demanding on the non-linear solver, and constraint equations originally used in arc-length methods proved not sufficiently robust [5, 6, 17].

For problems involving damage and plasticity the dissipation-based arc-length method [7, 8] seems to be the most robust method currently available. Yet, it suffers from the need to switch (back) to a force control when there is no energy dissipation. This deficiency has been solved in the approach presented here, where the method automatically switches between a control by the rate of the dissipated energy and the rate of the internal energy. The method requires only two parameters, making it simple to use, and has been applied to two examples involving fracture without any need for user intervention.

Appendix A. SHERMAN-MORRISON formula

The inverse of the matrix in Eq. (7)

$$\underline{\underline{\mathbf{K}}}_T = \begin{bmatrix} \underline{\underline{\mathbf{K}}} & -\underline{\hat{f}} \\ \underline{v}^T & w \end{bmatrix} \tag{A.1}$$

can be obtained as follows. Rewriting Eq. (A.1) gives

$$\underline{\underline{K}}_T = \begin{bmatrix} \underline{\underline{K}} & \mathbf{0} \\ \underline{\mathbf{0}}^T & 1 \end{bmatrix} - \underline{x}_1 \underline{y}_1^T - \underline{x}_2 \underline{y}_2^T = \underbrace{\underline{\underline{A}} - \underline{\underline{A}}_1}_{\underline{\underline{B}}} - \underline{\underline{A}}_2 \tag{A.2}$$

with

$$\underline{x}_1 = \begin{bmatrix} \hat{\underline{f}} \\ 0 \end{bmatrix}, \qquad \underline{y}_1^T = \begin{bmatrix} \underline{\mathbf{0}}^T & 1 \end{bmatrix} \qquad \rightarrow \underline{x}_1 \underline{y}_1^T = \begin{bmatrix} \underline{\mathbf{0}} & \hat{\underline{f}} \\ \underline{\mathbf{0}}^T & 0 \end{bmatrix}, \tag{A.3}$$

$$\underline{x}_2 = \begin{bmatrix} \underline{\mathbf{0}} \\ -1 \end{bmatrix}, \qquad \underline{y}_2^T = \begin{bmatrix} \underline{v}^T & w - 1 \end{bmatrix} \qquad \rightarrow \underline{x}_2 \underline{y}_2^T = \begin{bmatrix} \underline{\mathbf{0}} & \mathbf{0} \\ -\underline{v}^T & 1 - w \end{bmatrix}. \tag{A.4}$$

Application of the SHERMAN-MORRISON formula yields the following expressions

$$\underline{\underline{K}}_T^{-1} = \left(\underline{\underline{B}} - \underline{\underline{A}}_2 \right)^{-1} = \left(\underline{\underline{B}} - \underline{x}_2 \underline{y}_2^T \right)^{-1} = \underline{\underline{B}}^{-1} + \frac{\underline{\underline{B}}^{-1} \underline{x}_2 \underline{y}_2^T \underline{\underline{B}}^{-1}}{1 - \underline{y}_2^T \underline{\underline{B}}^{-1} \underline{x}_2}, \tag{A.5}$$

$$\underline{\underline{B}}^{-1} = \left(\underline{\underline{A}} - \underline{\underline{A}}_1 \right)^{-1} = \left(\underline{\underline{A}} - \underline{x}_1 \underline{y}_1^T \right)^{-1} = \underline{\underline{A}}^{-1} + \frac{\underline{\underline{A}}^{-1} \underline{x}_1 \underline{y}_1^T \underline{\underline{A}}^{-1}}{1 - \underline{y}_1^T \underline{\underline{A}}^{-1} \underline{x}_1}, \tag{A.6}$$

while the terms in Eq. (A.6) can be expressed as

$$\underline{\underline{A}}^{-1} = \begin{bmatrix} \underline{\underline{K}}^{-1} & \mathbf{0} \\ \underline{\mathbf{0}}^T & 1 \end{bmatrix}, \quad \underline{\underline{A}}^{-1} \underline{x}_1 = \begin{bmatrix} \underline{\underline{K}}^{-1} \hat{\underline{f}} \\ 0 \end{bmatrix}, \quad \underline{y}_1^T \underline{\underline{A}}^{-1} = \begin{bmatrix} \underline{\mathbf{0}}^T & 1 \end{bmatrix}, \tag{A.7}$$

$$\underline{\underline{A}}^{-1} \underline{x}_1 \underline{y}_1^T \underline{\underline{A}}^{-1} = \begin{bmatrix} \underline{\mathbf{0}} & \underline{\underline{K}}^{-1} \hat{\underline{f}} \\ \underline{\mathbf{0}}^T & 0 \end{bmatrix}, \quad \underline{y}_1^T \underline{\underline{A}}^{-1} \underline{x}_1 = 0, \tag{A.8}$$

$$\underline{\underline{B}}^{-1} = \begin{bmatrix} \underline{\underline{K}}^{-1} & \mathbf{0} \\ \underline{\mathbf{0}}^T & 1 \end{bmatrix} + \begin{bmatrix} \underline{\mathbf{0}} & \underline{\underline{K}}^{-1} \hat{\underline{f}} \\ \underline{\mathbf{0}}^T & 0 \end{bmatrix} \tag{A.9}$$

and in Eq. (A.5) as

$$\underline{\underline{B}}^{-1} \underline{x}_2 = \begin{bmatrix} -\underline{\underline{K}}^{-1} \hat{\underline{f}} \\ -1 \end{bmatrix}, \quad \underline{y}_2^T \underline{\underline{B}}^{-1} = \begin{bmatrix} \underline{v}^T \underline{\underline{K}}^{-1} & \underline{v}^T \underline{\underline{K}}^{-1} \hat{\underline{f}} + w - 1 \end{bmatrix}, \tag{A.10}$$

$$\underline{\underline{B}}^{-1} \underline{x}_2 \underline{y}_2^T \underline{\underline{B}}^{-1} = \begin{bmatrix} -\underline{\underline{K}}^{-1} \hat{\underline{f}} \underline{v}^T \underline{\underline{K}}^{-1} & -\underline{\underline{K}}^{-1} \hat{\underline{f}} \underline{v}^T \underline{\underline{K}}^{-1} \hat{\underline{f}} - w \underline{\underline{K}}^{-1} \hat{\underline{f}} + \underline{\underline{K}}^{-1} \hat{\underline{f}} \\ -\underline{v}^T \underline{\underline{K}}^{-1} & -\underline{v}^T \underline{\underline{K}}^{-1} \hat{\underline{f}} - w + 1 \end{bmatrix}, \tag{A.11}$$

$$\underline{y}_2^T \underline{\underline{B}}^{-1} \underline{x}_2 = -\underline{v}^T \underline{\underline{K}}^{-1} \hat{\underline{f}} - w + 1. \tag{A.12}$$

With

$$\underline{q} = \underline{\underline{K}}^{-1} \hat{\underline{f}} \quad \text{and} \quad \underline{q} = \frac{\underline{q}(\underline{v}^T \underline{q} + w)}{\underline{v}^T \underline{q} + w} = \frac{\underline{q} \underline{v}^T \underline{q} + w \underline{q}}{\underline{v}^T \underline{q} + w} \tag{A.13}$$

13

Eq. (A.1) becomes

$$\underline{\underline{\mathbf{K}}}_T^{-1} = \begin{bmatrix} \underline{\underline{\mathbf{K}}}^{-1} & \mathbf{0} \\ \mathbf{0}^T & 1 \end{bmatrix} + \begin{bmatrix} \underline{\underline{\mathbf{0}}} & \underline{q} \\ \underline{0}^T & 0 \end{bmatrix} + \frac{\begin{bmatrix} -\underline{q}\underline{v}^T\underline{\underline{\mathbf{K}}}^{-1} & -\underline{q}\underline{v}^T\underline{q} - w\underline{q} + \underline{q} \\ -\underline{v}^T\underline{\underline{\mathbf{K}}}^{-1} & -\underline{v}^T\underline{q} - w + 1 \end{bmatrix}}{\underline{v}^T\underline{q} + w} \tag{A.14}$$

$$= \begin{bmatrix} \underline{\underline{\mathbf{K}}}^{-1} & \mathbf{0} \\ \underline{0}^T & 1 \end{bmatrix} + \frac{\begin{bmatrix} \underline{\underline{\mathbf{0}}} & \underline{q}\underline{v}^T\underline{q} + w\underline{q} \\ \underline{0}^T & 0 \end{bmatrix} + \begin{bmatrix} -\underline{q}\underline{v}^T\underline{\underline{\mathbf{K}}}^{-1} & -\underline{q}\underline{v}^T\underline{q} - w\underline{q} + \underline{q} \\ -\underline{v}^T\underline{\underline{\mathbf{K}}}^{-1} & -\underline{v}^T\underline{q} - w + 1 \end{bmatrix}}{\underline{v}^T\underline{q} + w} \tag{A.15}$$

$$= \begin{bmatrix} \underline{\underline{\mathbf{K}}}^{-1} & \mathbf{0} \\ \underline{0}^T & 1 \end{bmatrix} + \frac{1}{\underline{v}^T\underline{q} + w} \begin{bmatrix} -\underline{q}\underline{v}^T\underline{\underline{\mathbf{K}}}^{-1} & \underline{q} \\ -\underline{v}^T\underline{\underline{\mathbf{K}}}^{-1} & -\underline{v}^T\underline{q} - w + 1 \end{bmatrix}. \tag{A.16}$$

Appendix B. Time discretisation scheme for the arc-length control

For the initial-value problem with $t \in [0, T]$

$$\dot{x}(t) = f(x(t)) \tag{B.1}$$
$$x(0) = x_n \tag{B.2}$$

the generalised midpoint rule is defined as follows [18]

$$f(x_{n+\theta}) = \frac{x_{n+1} - x_n}{\Delta t}, \quad x_{n+\theta} = \theta x_{n+1} + (1 - \theta)x_n, \quad \theta \in [0, 1] \tag{B.3}$$

with $\theta = 0$ for forward EULER, $\theta = \frac{1}{2}$ for midpoint rule and $\theta = 1$ for backward EULER. x_{n+1} and x_n denote in Eq. (B.3) the solution for the variable x at time increment $n+1$ and n, respectively.

Appendix B.1. Time discretisation for the rate of internal energy
Applying the time discretisation scheme in Eq. (B.3) to Eq. (23)

$$\frac{1}{2}\left(\underline{\dot{u}}^T \lambda + \underline{u}^T \dot{\lambda}\right)\underline{\hat{f}} - \dot{\tau}^U = 0 \tag{B.4}$$

gives

$$\frac{1}{2}\Bigg((\theta\lambda_{n+1} + (1 - \theta)\lambda_n)\frac{\underline{u}_{n+1}^T - \underline{u}_n^T}{\Delta t}$$
$$+ \frac{\lambda_{n+1} - \lambda_n}{\Delta t}(\theta\underline{u}_{n+1}^T + (1 - \theta)\underline{u}_n^T)\Bigg)\underline{\hat{f}} - \frac{\tau_{n+1}^U - \tau_n^U}{\Delta t}$$
$$= \frac{1}{2}\Bigg(2\theta\frac{\lambda_{n+1}\underline{u}_{n+1}^T}{\Delta t} + (1 - 2\theta)\frac{\lambda_{n+1}\underline{u}_n^T}{\Delta t}$$
$$+ (1 - 2\theta)\frac{\lambda_n\underline{u}_{n+1}^T}{\Delta t} + (2\theta - 2)\frac{\lambda_n\underline{u}_n^T}{\Delta t}\Bigg)\underline{\hat{f}} - \frac{\Delta\tau^U}{\Delta t} = 0. \tag{B.5}$$

Using the midpoint rule with $\theta = \frac{1}{2}$ in Eq. (B.5) yields the arc-length function φ^U

$$\varphi^U(\underline{u}_{n+1}, \lambda_{n+1}) = \frac{1}{2}\left(\lambda_{n+1}\underline{u}_{n+1}^T - \lambda_n\underline{u}_n^T\right)\underline{\hat{f}} - \Delta\tau^U. \tag{B.6}$$

14

Appendix B.2. Time discretisation for the rate of dissipated energy

Starting with the constraint equation from Eq. (20)

$$\frac{1}{2}(\lambda\dot{\underline{u}}^T - \dot{\lambda}\underline{u}^T)\hat{\underline{f}} - \dot{\tau}^D = 0 \tag{B.7}$$

and application of Eq. (B.3) gives

$$\frac{1}{2}\Big((\theta\lambda_{n+1} + (1-\theta)\lambda_n)\frac{\underline{u}_{n+1}^T - \underline{u}_n^T}{\Delta t}$$
$$- \frac{\lambda_{n+1} - \lambda_n}{\Delta t}(\theta\underline{u}_{n+1}^T + (1-\theta)\underline{u}_n^T)\Big)\hat{\underline{f}} - \frac{\tau_{n+1}^D - \tau_n^D}{\Delta t}$$
$$= \frac{1}{2}\left(\frac{\lambda_n\underline{u}_{n+1}^T}{\Delta t} - \frac{\lambda_{n+1}\underline{u}_n^T}{\Delta t}\right)\hat{\underline{f}} - \frac{\Delta\tau^D}{\Delta t} = 0. \tag{B.8}$$

Therefore, the arc-length function φ^D for *any* time discretisation scheme can be written as

$$\varphi^D(\underline{u}_{n+1}, \lambda_{n+1}) = \frac{1}{2}\left(\lambda_n\underline{u}_{n+1}^T - \lambda_{n+1}\underline{u}_n^T\right)\hat{\underline{f}} - \Delta\tau^D. \tag{B.9}$$

References

[1] Wempner, G. A.: *Discrete approximations related to nonlinear theories of solids*; International Journal of Solids and Structures; **7**; 1581–1599; 1971

[2] Riks, E.: *An incremental approach to the solution of snapping and buckling problems*; International Journal of Solids and Structures; **15**; 529–551; 1979

[3] Crisfield, M. A.: *A fast incremental/iterative solution procedure that handles "snap-through"*; Computers & Structures; **13**; 55–62; 1981

[4] Ramm, E.: *Strategies for tracing ther nonlinear response near limit points*; in Wunderlich, W.; Stein, E.; Bathe, K. J., editors, *Nonlinear finite element analysis in Structural Mechanics* Springer

[5] Crisfield, M. A.: *Local instabilities in the non-linear analysis of reinforced concrete beams and slabs*; Institution of Civil Engineers, Proceedings; **73**; 135–145; 1982

[6] de Borst, R.: *Computation of post-bifurcation and post-failure behavior of strain-softening solids*; Computers & Structures; **25**; 211–224; 1987

[7] Gutiérrez, M. A.: *Energy release control for numerical simulations of failure in quasi-brittle solids*; Communications in Numerical Methods in Engineering; **20**; 19–29; 2004

[8] Verhoosel, C. V.; Remmers, J. J. C.; Gutiérrez, M. A.: *A dissipation-based arc-length method for robust simulation of brittle and ductile failure*; International Journal for Numerical Methods in Engineering; **77**; 1290–1321; 2009

[9] Jiràsek, M.; Bazant, Z. P.: *Inelastic Analysis of Structures*; Wiley; 2001

[10] Miehe, C.; Hofacker, M.; Welschinger, F.: *A phase field model for rate-independent crack propagation: Robust algorithmic implementation based on operator splits*; Computer Methods in Applied Mechanics and Engineering; **199**; 2765–2778; 2010

[11] Lorentz, E.; Badel, P.: *A new path-following constraint for strain-softening finite element simulations*; International Journal for Numerical Methods in Engineering; **60**; 499–526; 2004

[12] Amor, H.; Marigo, J.-J.; Maurini, C.: *Regularized formulation of the variational brittle fracture with unilateral contact: Numerical experiments*; Journal of the Mechanics and Physics of Solids; **57 (8)**; 1209–1229; 2009

[13] Borden, M. J.; Verhoosel, C. V.; Scott, M. A.; Hughes, T. J.; Landis, C. M.: *A phase-field description of dynamic brittle fracture*; Computer Methods in Applied Mechanics and Engineering; **217–220 (0)**; 77–95; 2012

[14] May, S.; Vignollet, J.; de Borst, R.: *A numerical assessment of phase-field models for brittle and cohesive fracture: Γ-Convergence and stress oscillations*; European Journal of Mechanics-A/Solids; **52**; 72–84; 2015

[15] Schellekens, J. C. J.; de Borst, R.: *On the numerical integration of interface elements*; International Journal for Numerical Methods in Engineering; **36**; 43–66; 1993

[16] Vignollet, J.; May, S.; de Borst, R.: *On the numerical integration of isogeometric interface elements*; International Journal for Numerical Methods in Engineering; 2015

[17] de Borst, R.; Crisfield, M. A.; Remmers, J. J. C.; Verhoosel, C. V.: *Nonlinear Finite Element Analysis of Solids and Structures*; Wiley; 2012

[18] Simo, J. C.; Hughes, T. J. R.: *Computational Inelasticity*; Springer; 1998